Microparticles decorated with cell-instructive surface chemistries actively promote wound healing

Arsalan Latif, Leanne E Fisher, Adam A Dundas, Valentina Cuzzucoli Crucitti, Zeynep Imir, Karen Lawler, Francesco Pappalard, Benjamin W Muir, Ricky Wildman, Derek J. Irvine*, Morgan R Alexander*, Amir M Ghaemmaghami*

A. Latif, L. E. Fisher, K. Lawler, A. M. Ghaemmaghami

School of Life Sciences, University of Nottingham, NG7 2RD, United Kingdom

Email: amir.ghaemmaghami@nottingham.ac.uk

A. D. Dundas, V. Cuzzucoli Crucitti, R. Wildman, D. J. Irvine

Faculty of Engineering, University of Nottingham, NG7 2RD, United Kingdom

Email: derek.irvine@nottingham.ac.uk

Z. Imir, F. Pappalardo, M. R. Alexander

School of Pharmacy, University of Nottingham, NG7 2RD, United Kingdom

Email: morgan.alexander@nottingham.ac.uk

WILEY-VCH

B. W. Muir

Commonwealth Scientific & Industrial Research Organization, Australia

Abstract

Wound healing is a complex biological process involving close crosstalk between various cell types. Dysregulation in any of these processes, such as in diabetic wounds, results in chronic non-healing wounds. Fibroblasts are a critical cell type involved in the formation of granulation tissue, essential for effective wound healing. We screened 315 different polymer surfaces to identify candidates which actively drove fibroblasts towards either pro- or anti-proliferative functional phenotypes. Fibroblast-instructive chemistries were identified, which we synthesized into surfactants to fabricate easy to administer microparticles for direct application to diabetic wounds. The pro-proliferative microfluidic derived particles were able to successfully promote neovascularisation, granulation tissue formation and wound closure after a single application to the wound bed. These active novel 3D bio-instructive microparticles show great potential as a route to reducing the burden of chronic wounds.

1. Introduction

Wound healing is a complex biological process that involves close crosstalk between structural, stromal and immune cells.[1, 2] It consists of four overlapping sequential phases, each having defined

WILEY-VCH

cell signaling and biochemical events. Following injury, the haemostasis phase results in the formation of a scaffold for infiltrating cells, while acting as a reservoir of growth factors and cells. The inflammatory phase that follows is characterized by infiltration of immune cells that phagocytose cell debris and microbes, and secrete cytokines to instigate the proliferative phase. Proliferation and migration of fibroblasts, myofibroblasts and endothelial cells forms granulation tissue in which fibroblasts are the most prevalent cell type. Fibroblasts secrete structural extracellular matrix (ECM) components and act to remodel the ECM to form mature scar tissue or regenerated skin in the final phase of wound healing: the remodelling phase. During the inflammatory and proliferative phase, fibroblasts also secrete an array of cytokines, chemokines, and growth factors that regulate the cellular microenvironment via autocrine and paracrine signaling. The balance between these processes determines the outcome of wound healing, in particular fibrosis, scar tissue formation and regeneration of the wound.[3-5]

Chronic non-healing wounds such as diabetic wounds exhibit dysregulated healing. They exhibit a prolonged inflammatory phase, and a failed transition to the proliferative phase which consequently induces persistent inflammation.[6] Moreover, cells within the diabetic wound microenvironment exhibit dysregulated production of pro- and anti-inflammatory cytokines, and impaired angiogenesis.[7, 8] Specifically, fibroblasts within the diabetic wound exhibit unwanted phenotypes and behaviors which are marked by diminished ECM synthesis and decreased proliferative and migratory ability.[7, 9] This then hinders the formation of granulation tissue.

To address this, we propose to positively modulate the fibroblast phenotype and behavior via the development of active bio-instructive stromal cell instructive materials, with the ultimate goal of promoting diabetic wound healing. This is informed by previous studies[10-13] that have shown changes in the physiochemical properties of biomaterials can influence stromal cell behavior: specifically, cell attachment, proliferation, differentiation, and migration. In the absence of sufficient knowledge to design chemical cues to modulate fibroblast phenotype and function, a high-throughput approach that allowed examination of a wide chemical space was chosen. High-

WILEY-VCH

throughput screening of combinatorial polymer libraries has previously led to the discovery of polymers that modulate macrophage phenotype, instruct pluripotent stem cell expansion and differentiation and suppress bacterial biofilm formation.[14-16] It was therefore hypothesized that a polymer with potential for inducing fibroblast instructive ques to modulate cells towards a pro-proliferative phenotype and behavior could be discovered within a chemically diverse library of polymers. This hypothesis was examined by screening a polymer micro array library of meth(acrylate) and acrylamide polymers for fibroblast-instructive chemistries that controlled proliferation and differentiation. To translate the discovered pro- and anti-proliferative chemistries into a delivery system suitable for wound treatment, they were synthesized into surfactants and fabricated into microparticles using droplet microfluidics.[17, 18] Microparticle based therapeutic delivery systems avoid invasive surgical procedures by achieving injectability and aggregation *in situ.*[19, 20] The resultant pro- and anti-proliferative microparticles were then studied in a series of *in vitro* and *in vivo* models for their ability to modulate fibroblast phenotype and accelerate diabetic wound healing.

2. Results and Discussion

2.1 Discovery of fibroblast instructive polymers

For a material to promote wound healing, chemical cues must instruct fibroblasts to attach, spread and proliferate whilst controlling differentiation into myofibroblasts. Fibroblast attachment, morphology, proliferation, and differentiation was measured on a 315 member combinatorial polymer library using automated high content optical microscopy (Table S1). The monomer library was developed to create the widest polymer chemical space that can be put together using commercially available monomers. The (meth)acrylate and (meth)acrylamides are photo-polymerizable monomers with a range of pendant group molecular moieties including linear,

branched, cyclic, aromatic structures. They also include monomers with non-hydrocarbon hetero-group functionalities. Monomers were printed using a dispensing station via metal pins onto epoxy coated slides dip coated with poly (2-hydroxyethyl methacrylate) (pHEMA) to achieve 945 spots of ~ 300μm in diameter. Three replicate spots of each polymer were printed on each slide, with multiple slides being tested to give biological replicates.

Fibroblasts cultured on polymer spots were grouped into anti-attachment (cell count less than 10 cells per spot), low attachment (cell numbers between 10 and tissue culture plastic (TCP) cell attachment controls), and pro-attachment polymers (cell numbers per spot greater than TCP controls) (Figure S1). Whilst TCP may not be neutral in its cell response, TCP is universally used for cell culture and serves as a good benchmark to assess the impact of other substrates in controlling cell behavior. Fibroblast morphology varied across the polymer microarray from elongated spindle-like morphologies to rounded morphology (Figure S2). Fibroblasts with a rounded morphology are indicative of a lack of spreading thereby hindering cellular functionality.[21] The fibroblasts also ranged in size on the polymers from 5 - 175 (% area normalized to TCP) (**Figure 1**a), and while certain polymers promoted the adhesion of many cells, the same polymers did not necessarily support greater cell spreading (Figure S2). To identify polymers that supported cell attachment and spreading, a threshold of at least 20 adherent cells (per spot) with an area greater than 60% of those on TCP was applied. The 20 adherent cells per spot attachment threshold is equivalent to approximately 2500 cells/cm^2 and corresponds with what we had identified in our optimization experiments as the lower end of cell density that supports confluency over 3 days when cells are cultured on tissue culture plastic.
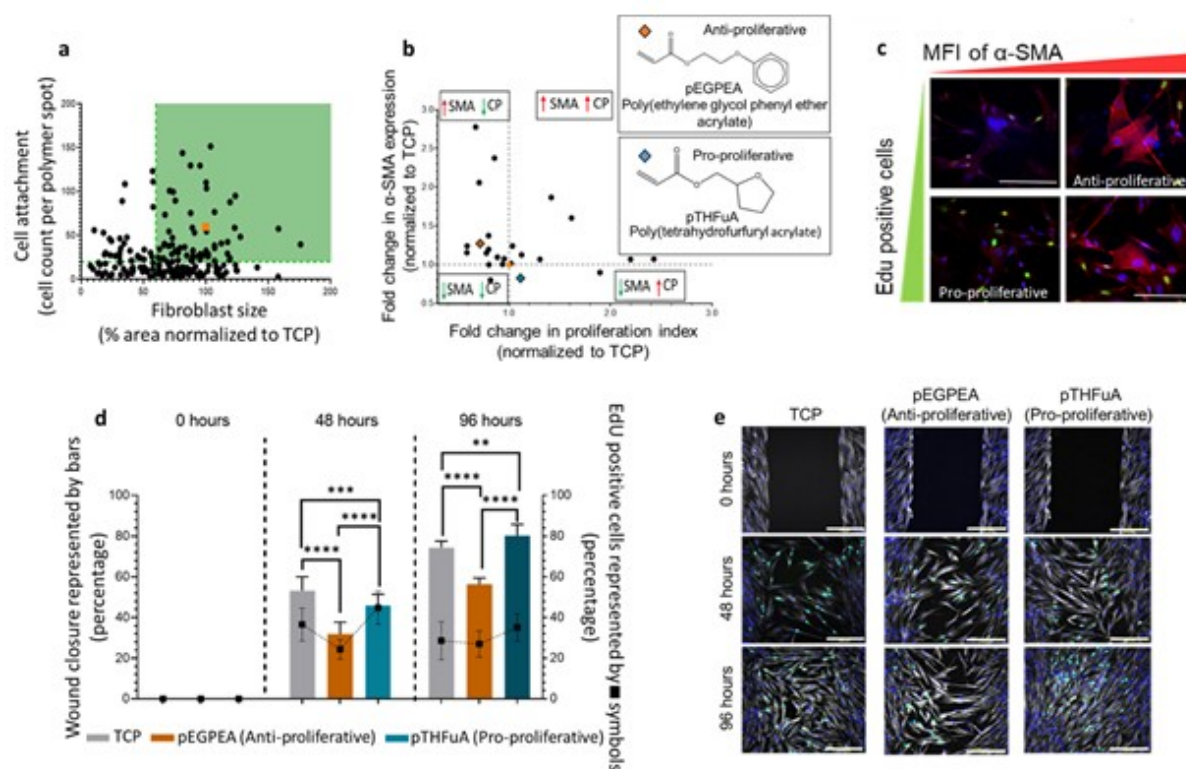
Figure 1. Discovery of polymers that modulate fibroblast phenotype. a) Number of adherent cells on polymer spots plotted against fibroblast size (% area normalized to TCP control). The orange data point represents TCP control. All polymers within the green zone (cut off 20 cells per polymer spot and 60% cell size) and meeting a signal to noise (SNR) > 3 criterion were selected for phenotypic studies. N=2, n=12. b) Grouping of polymers into quadrants based on modulation of expression of α-SMA and proliferation, relative to TCP (orange data point). The red data point represents TCP (+TGF-β1). Pro-proliferative (pTHFuA) and anti-proliferative (pEGPEA) polymers were chosen based on their ability to control fibroblast differentiation and proliferation. c) Fluorescent images of EdU positive cells (green), α-SMA (red) and nuclei (blue). Scale bar = 100 μm. d) Percent wound closure by fibroblasts cultured on TCP controls, anti-proliferative and pro-proliferative polymers for various culture time. The square data points within bar graph represent percent EdU positive cells within wound. The pro-proliferative substrate (pTHFuA) accelerated wound closure and had highest percent EdU positive cells. e) Fluorescent images of cells stained for α-tubulin (gray), EdU positive cells (cyan) and nuclei (blue). Scale bars = 100 μm. N=2, n=6 ±SD. Statistical significance was

calculated using one-way ANOVA and the Tukey's post hoc analysis where $*p < 0.1$, $**p < 0.01$, $***p < 0.001$, $****p < 0.0001$.

The functional phenotype of fibroblasts on polymers supporting attachment and spreading was determined using proliferation assays expressed as a proliferative index, and fibroblast differentiation into α-SMA expressing myofibroblasts measured via mean fluorescence intensity (MFI). To understand the effects of the polymers on fibroblast proliferation and differentiation, the fold change in proliferative index and α-SMA expression (with respect to TCP) was plotted and is shown in Figure 1b. This enabled visualization of the phenotypic modulatory ability of the polymers relative to the TCP control. Based on this understanding, the polymers were classified into four groups constructed from their quadrant locations in a cell proliferation and α-SMA expression plot. It was also observed that fibroblasts cultured on TCP and stimulated with TGF-β1 (a positive acting control) induced proliferation and differentiation (fold change of 2.5 and 2.2 respectively), as studied previously [22-24] (Figure S3). Moreover, poly(tetrahydro furfuryl acrylate) (pTHFuA) promoted proliferation and suppressed differentiation (fold change of 1.11 and 0.82, respectively) whereas poly(ethylene glycol phenyl ether acrylate) (pEGPEA) suppressed proliferation and promoted differentiation (fold change of 0.71 and 1.27, respectively). Both proliferation and differentiation are phenotypic traits that are crucial in determining the outcome of wound healing. α-SMA as a marker for fibroblast differentiation to myofibroblasts was used in this study as a surrogate for fibrotic behavior. Myofibroblasts are key cell types involved in wound healing, the persistent presence of which has been linked to scarred healing.[25] Whilst fibroblast proliferation is vital for formation of granulation tissue, balancing fibroblast differentiation ensures effective wound remodelling. Additionally, pTHFuA and pEGPEA were selected from the high throughput screening because a) they had a low coefficient of variation (COV), thus high reproducibility, b) they could be polymerized using thermal free radical polymerization and c) they could be synthesized into surfactants for fabrication into microparticles (i.e. polymers that inherently crosslinked were removed). Thus, polymers that may have shown higher fold change in proliferative index or α-SMA expression represented an inability to be synthesized into surfactants and thus microparticles and/or

showed a higher COV, lowering reproducibility. We will therefore designate pTHFuA as a pro-proliferative polymer and pEGPEA as an anti-proliferative polymer.

2.2. Functional phenotype assays confirm the discovery of fibroblast-instructive chemistries

pTHFuA pro-proliferative and pEGPEA anti-proliferative polymers were polymerized and spin coated onto 13 mm diameter glass cover slips in order to give a larger area of polymer to conduct functional phenotype assays. The functional phenotype of fibroblasts were confirmed by proliferation studies using EdU, and α-SMA expression (Figure S3). Fibroblasts cultured on the pro-proliferative polymer had 2-fold more EdU positive cells than fibroblasts cultured on anti-proliferative polymer surfaces. Similarly, cells cultured on anti-proliferative polymers had 2-fold higher expression of α-SMA than those cultured on pro-proliferative polymers. The data confirmed polymers at the macro-scale mediate fibroblast behavior towards distinct wound regeneration profiles.

2.3. Pro-proliferative and anti-proliferative surfaces regulate wound closure in an *in vitro* wound healing assay

A scratch assay was performed to investigate wound closure on the anti-proliferative and pro-proliferative polymer surfaces. After 48 hours, fibroblasts on the pro-proliferative surface had encroached on 48% of the initial 'wound' area compared to 35% on the anti-proliferative surface (Figure 1d and e). At 96 hours, the pro-proliferative surfaces conferred an 82% wound closure compared to 55% on the anti-proliferative surface. This observation demonstrates the functional ability of the pro-proliferative polymer to accelerate fibroblast proliferation and migration bringing about wound healing.

WILEY-VCH

2.4. Microparticle fabrication and characterization

Polymer microparticles with the pro- and anti-proliferative surface chemistries were used as the format to stimulate bio-instructive stromal cell niches in a wound environment. Microparticles were made using a droplet microfluidic process to achieve uniform particle sizes. Commercial surfactants, such as poly(vinyl alcohol-co-vinyl acetate) (PVA), are commonly used to form stable emulsions[26] but they inevitably contaminate the surface of materials which can affect cell-surface interactions. We therefore investigated the use of surfactants that offer the desired surface bio-stimulatory functionality, termed surfmers[18, 27], by synthesising THFuA-*co*-poly(ethylene glycol) methyl ether methacrylate (mPEGMA) and EGPEA-*co*-mPEGMA polymers as pro- and anti-proliferative surfactants, respectively. The mPEGMA component acts as the hydrophilic component to stabilize the production of a hydrophobic polymer particle using aqueous UV photo-polymerization in a microfluidic system. This enabled the surfactant to be used in the dispersed phase with the monomer and photoinitiator, whilst keeping the continuous phase as purely DI water. The emulsion micelles produced in the microfluidic device were then irradiated with UV light upon collection to cure the dispersed (which has become the emulsion micelles core) phase and form the functionalized microparticles. The core material used to produce the microparticles is 1,6 hexanediol diacrylate, making the particles non-degradable. This simpler non-resorbable system enables investigating the bio-instructive potential of the surface chemistry in the absence of the complexity of biosorption during *in vivo* experimentation. To investigate the surface, microparticles were characterized using Scanning electron microscopy (SEM) and Time of flight - Secondary ion mass spectrometry (ToF-SIMS) as shown in **Figure 2**.
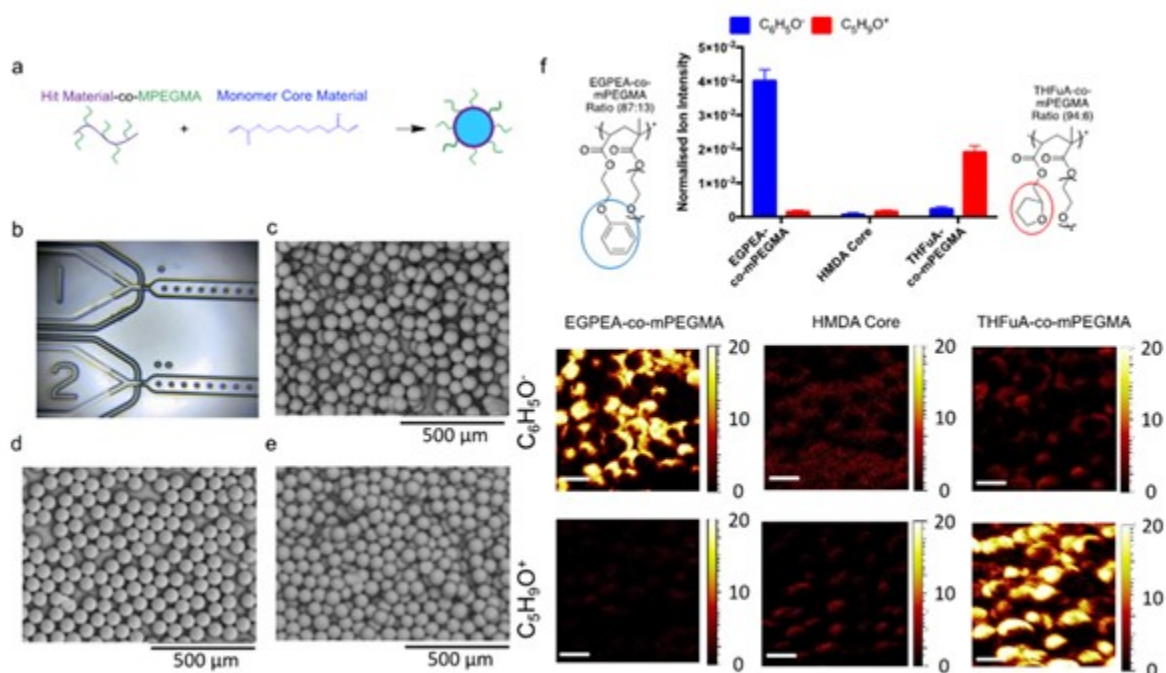
Figure 2. a) Polymer microparticles with chosen surface chemistry produced using an emulsion polymerization technique with synthesized polymer surfactants and a diacrylate core material. b) Particles are produced using a scale-out (7-junction) droplet microfluidics approach to ensure sufficient monodisperse quantities are manufactured. c) SEM image of polymer particles produced with a THFuA-co-mPEGMA surfactant with a size of 71.9 ± 2.5 μm (COV) = 3.4%). d) SEM image of polymer particles produced with an EGPEA-co-mPEGMA surfactant with a size of 73.0 ± 1.5 μm (COV = 3.0%). e) SEM image of polymer particles produced with no surfactant with a size of 69.4 ± 3.3 μm (COV = 4.8%). f) Tof-SIMS data showing the identification of unique ions for EGPEA ($C_6H_5O^-$) and THFuA ($C_5H_9O^+$) on polymer microparticles with associated chemical image maps. Particles were compared against polymer particles made from the same core-material but without a surfactant to confirm that surfactants had been successfully placed on the surface of microparticles. *N*=3 regions of interest used, scale bars = 100 μm.

SEM images revealed particles with diameters of 71.9 ± 2.5 μm, 73.0 ± 1.5 μm and 69.4 ± 3.3 μm for those with surfmers THFuA-co-mPEGMA (pro-proliferative), EGPEA-co-mPEGMA (anti-proliferative)

10

WILEY-VCH

and without respectively. All calculated COV for the particles were below 5%, confirming the particles were monodisperse.[28, 29] The particles with no surfmer had the largest variation at 4.8%, consistent with there being no surfactant to stabilize the interface. The COV for microparticles with polymer surfactants, 3.4 % for THFuA-co-mPEGMA and 3.0% for EGPEA-co-mPEGMA), demonstrates that the surfactant is stabilizing the surface effectively when compared to the particles without surfactant. Determination of the surface chemistry was performed using ToF-SIMS. The unique ions of $C_5H_9O^+$ and $C_6H_5O^-$ were used to identify the chemical structures of THFuA and EGPEA respectively. In comparison to microparticles with no surfactant, it was clear the surfaces of each particle were decorated with the desired surface chemistry, which is demonstrated both by the normalized ion intensities and the chemical map images in Figure 2f. To confirm the chemistry on the surfaces remained, functionalized and non-functionalized particles were incubated in DI water at 37°C for 21 days and analyzed again using ToF-SIMS. No significant change in the surface chemistry was observed (Figure S4).

2.5. Bio-instructive microparticles promote wound healing fibroblast phenotype

Fibroblast adherence and viability on coated microparticles was studied by measuring the total cellular DNA content. Both pro- and anti-proliferative microparticles were shown to support high cell viability (Figure S5). Fibroblast proliferation was investigated by measuring the increase in cell number during a culture period of 24 to 96 hours (**Figure 3**a). Pro-proliferative microparticles had an approximate 3-fold increase in the number of attached fibroblasts compared to anti-proliferative microparticles (1.5-fold increase). To further characterize functional response of fibroblasts, cells cultured on pro- and anti-proliferative microparticles were studied for gene expression of ECM markers collagen I (α1) and collagen III (α1) using qPCR. This was due to the fact that fibroblasts are the primary cell types involved in the expression of both markers. Fibroblasts cultured on anti-proliferative microparticles upregulated both collagen I and collagen III, with a 7.1 and 13.5-fold increase in gene expression respectively (Figure 3c). Conversely, fibroblasts cultured on pro-proliferative microparticles had significantly lower collagen I and collagen III expression, by 6.3 and

10.0-fold respectively. Collagen III is the predominant variant in the early stages of wound healing and is gradually replaced by collagen I as healthy healing progresses. An increased collagen III:I ratio has been associated with the formation of scarred fibrotic wound healing opposed to a lower collagen III:I ratio which leads towards scarless healing.[30-32] For instance, in the case of incisional hernia, increased collagen III:I ratio resulted in impaired wound healing and reduced mechanical strength of the connective tissue[33], whereas low collagen III:I expression ratio of fetal fibroblasts has been associated with scarless wound healing.[34] These studies suggest that modulating the collagen III/I expression ratio may guide the outcome of wound healing. Thus, a lower collagen III:I ratio as observed with microparticles coated with the pro-proliferative polymer would suggest an anti-fibrotic scarless wound healing response.

WILEY-VCH
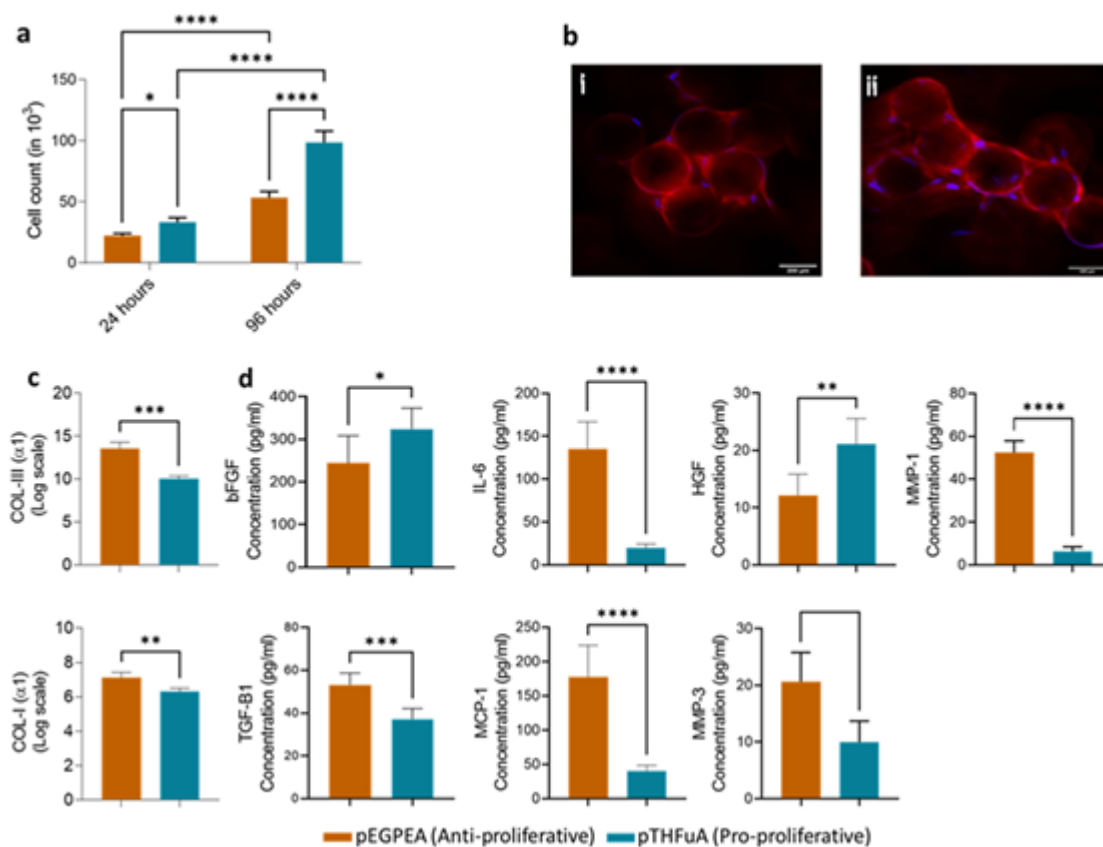
Figure 3. Fibroblast functional behavior and phenotype on wound-instructive microparticles. a) Fibroblast attachment on anti-proliferative (pEGPEA) and pro-proliferative (pTHFuA) microparticles at 24 and 96 hours. Cell proliferation was studied by correlating measured DNA content to the number of adherent cells at 24 and 96 hours of culture. b) Fibroblasts adherent on i) anti-proliferative (pEGPEA) and ii) pro-proliferative (pTHFuA) microparticles were stained for F-actin (Red) and nuclei (blue) to visualise cells. Scale bar = 200 μm. c) Gene expression of collagen III (α1) and collagen I (α1) of fibroblasts cultured on microparticles, using qPCR. d) A panel of cytokines and growth factors secreted by fibroblasts were studied to elucidate the effect of fibroblast-microparticle systems on the cellular microenvironment. Data shown is from the mean of N=2, n=6 ±SD. Statistical significance was calculated using one-way ANOVA and the Tukey's post hoc analysis where *p <0.1, **p<0.01, ***p<0.001, ****p<0.0001.

To steer wound healing towards functional tissue regeneration and remodelling, it is also important to study the autocrine and paracrine signaling microenvironment. This was quantified by measuring a panel of cytokines and growth factors using ELISA that covered both pro-proliferative and anti-proliferative factors (Figure 3d). Fibroblasts cultured on pro-proliferative microparticles had significantly higher concentrations of basic fibroblast growth factor (bFGF), and hepatocyte growth factor (HGF) compared to anti-proliferative microparticles. Conversely, cells cultured on anti-proliferative microparticles had significantly higher concentrations of TGF-β1, IL-6, MCP-1, MMP-1, and MMP-3. Both cytokine and growth factor profiles were in-line with the functional application of the microparticles. Cytokines secreted in the cellular microenvironment influence cell behavior and phenotype, such as proliferation and ECM secretion, which ultimately influence the outcome of wound healing. For instance, the autocrine effect of fibroblast secreted bFGF enhances proliferation. This is observed on fibroblasts cultured on pro-proliferative microparticles, where high concentrations of bFGF coincide with a higher proliferative index. Interestingly, the anti-fibrotic growth factor HGF is known to accelerate wound healing and prevent fibrosis by synergistically acting with bFGF to promote proliferation and modulating the effects of pro-fibrotic cytokine TGF-β1.[35] It was observed that fibroblasts cultured on pro-proliferative microparticles secreted higher concentrations of HGF and bFGF, corresponding with a lower collagen III:I ratio and decreased α-

13

SMA and TGF-β1 expression, underpinning a pro-proliferative anti-fibrotic response. The lower concentration of TGF-β in pro-proliferative microparticles is interesting. While in the context of acute wounds TGF-β is generally thought to promote wound healing, its role in chronic wounds is more complex with conflicting data implicating high levels of TGF-β in non-healing chronic wounds (e.g. diabetic wounds), or development of fibrosis rather than healing.[36-38] Thus, lower concentrations of TGF-β is likely to be beneficial in promoting healing in chronic wounds which is also in line with our *in vivo* data in this study. Additionally, both MMP-1 and MMP-3 are elevated in diabetic wounds and are known to delay wound healing by degrading collagens, limiting contraction and re-epithelialization.[39-42] However, the anti-proliferative microparticles upregulated gene expression of collagen I (α1) and III (α1), yet its effect on ECM composition may be offset by higher secretion of MMP-1 and -3; thus, delaying diabetic wound healing.

Fibroblasts and macrophages have been identified as two major cell types affecting the outcome of wound healing. The impact of fibroblast-mediated recruitment of macrophages through paracrine signaling was therefore investigated by studying concentrations of MCP-1 and IL-6. The former acts as a chemoattractant for monocytes while the latter upregulates the M-CSF receptor on monocytes furthering their differentiation into macrophages.[43] Our data shows fibroblasts cultured on anti-proliferative microparticles expressed higher concentrations of both MCP-1 and IL-6. In addition, we also found increased production of MMPs from fibroblasts cultured on anti-proliferative polymers. It is interesting that IL-6 secreted by fibroblast seems to be essential for upregulation of MMP-1 secreted by macrophages.[44]. This together with an upregulation in MCP-1 as a chemoattractant for monocytes, would be suggestive of the arrival of monocytes differentiating to M1-like macrophages at a wound site, thus contributing to an inflammatory environment.

2.6. Pro-proliferative and anti-proliferative microparticles influence diabetic wound healing *in vivo*

14

The healing of full-thickness excisional skin wounds on the flanks of diabetic mice in receipt of pro- and anti-proliferative functionalized particles were compared to wounds which received no treatment (**Figure 4**a). Whilst all wound areas decreased in size with time, application of the pro-proliferative microparticles reduced the wound area at a faster rate (Figure 4d). Interestingly, as opposed to the pro-proliferative microparticle distribution, H&E staining (Figure 4b) revealed how anti-proliferative microparticles within the wound void dissipated to the sides of the wound where granulation tissue can be seen however, the central part of the wound bed showed little in terms of granulation tissue depth (GTD) (Figure S6d) and immune cell infiltration (Figure 4d and e). Massons Trichrome staining (Figure 4c) and subsequent collagen thickness analysis (Figure 4e) showed addition of pro-proliferative microparticles to diabetic wounds led to increased collagen production and improved healing and regeneration compared to anti-proliferative particles and un-treated wounds. In line with this, the percentage of wounds displaying initiation of neo-dermal tissue formation (Figure S6c) was 100% from day 8 onwards in wounds with receipt of the pro-proliferative microparticles, compared to 25% and 0% by day 20 with placement of non-healing microparticles and untreated wounds respectively. Data with specifics on enhanced wound contraction and wound re-epithelialization in the presence of pro-proliferative microparticles are given in Figure S6a and b.
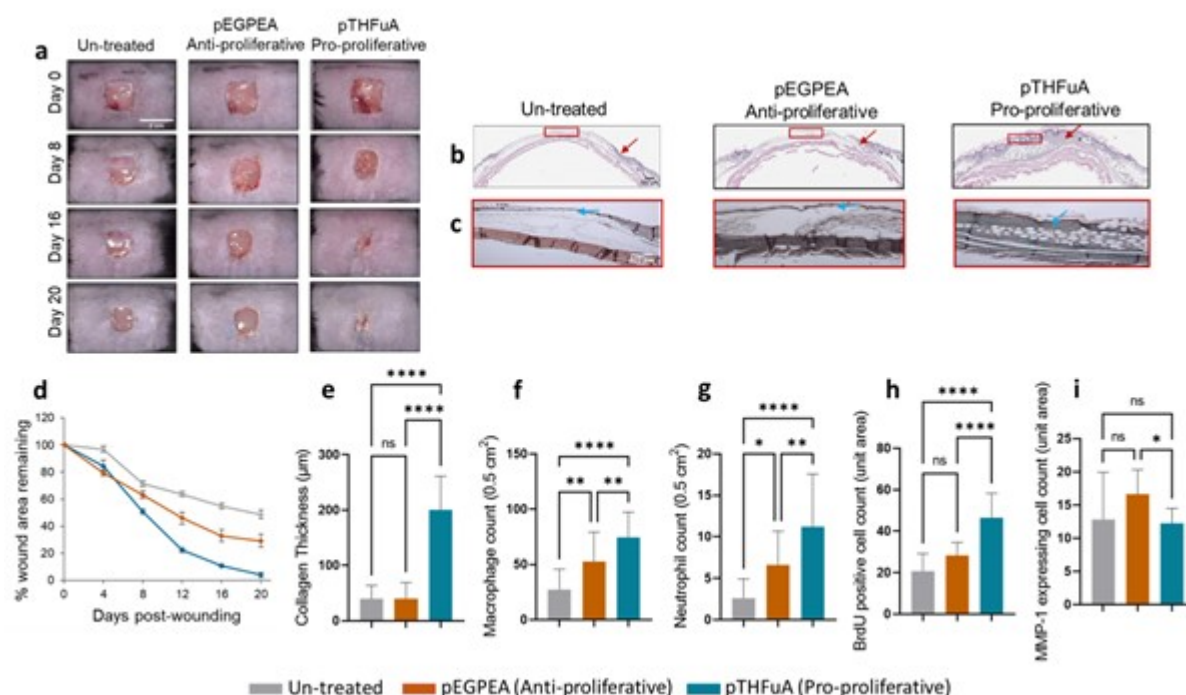
Figure 4. Histological results retrieved from diabetic mice with full thickness wounds exposed to anti-proliferative (pEGPEA) and pro-proliferative (pTHFuA) microparticles. Un-treated wounds served as a negative control. Scale bar = 2 cm. a) Photographs of wounds over time. b) Representative H&E images. Scale bar = 500 μm. c) Representative Massons Trichrome images showing differences in wound healing between treatments. Scale bar = 200 μm. d) Percentage wound area remaining (grey lines = un-treated wound, orange lines = anti-proliferative wounds, blue lines = pro-proliferative wounds), (e) Collagen thickness as determined by Massons trichrome staining. (f) macrophage count. g) neutrophil count. h) BrdU positive cell count (proliferative cells). i) MMP-1 expressing cell count. Red arrow = most advanced granulation tissue formation. Blue arrow = collagen thickness site. Representation of N=8 ±SEM for a-d and N=8 n=3-5 ±SD for e-i. Statistical significance was calculated using one-way ANOVA and the Tukey's post hoc analysis where *p <0.1, **p<0.01, ***p<0.001, ****p<0.0001.

It had been hypothesized that pro-proliferative microparticles may promote development of granulation tissue by accelerating cell proliferation[45-48], and expression of collagens within the

tissue microenvironment. Immunostaining for cell proliferation showed wounds treated with pro-proliferative microparticles had significantly more BrdU positive cells compared to anti-proliferative (p<0.0001) and untreated wounds (p<0.0001) (Figure 4h) and higher collagen I expression (**Figure 5**a). Interestingly, all wounds had similar levels of collagen III (Figure 5b). This indicated that the granulation tissue formed within wounds treated by pro-proliferative particles was predominantly formed of collagen I followed by collagen III, thereby up regulating the ratio of collagen I/III, which has been linked with enhanced diabetic wound healing in mice.[49] It has also been documented that fibroblast to myofibroblast differentiation throughout the healing process is dysregulated in diabetic mice.[50] We therefore performed immunostaining to detect α-SMA expression (Figure 5b). However, at day 21 there was no significant difference in diabetic wounds treated with pro- and anti-proliferative microparticles compared to wounds left un-treated. Additionally, diabetic wounds have been shown to have high concentrations of MMPs[39, 41, 42], and here we observe wounds treated with anti-proliferative microparticles had significantly higher MMP-1 positive cells compared to the pro-proliferative microparticle treatment (p=0.0473) (Figure 5i). The increased MMP-1 expression may have furthered collagen degradation thus reducing formation of collagen I and III matrices, cumulatively leading to a decrease in collagen thickness within the anti-proliferative intervention diabetic wound microenvironment.
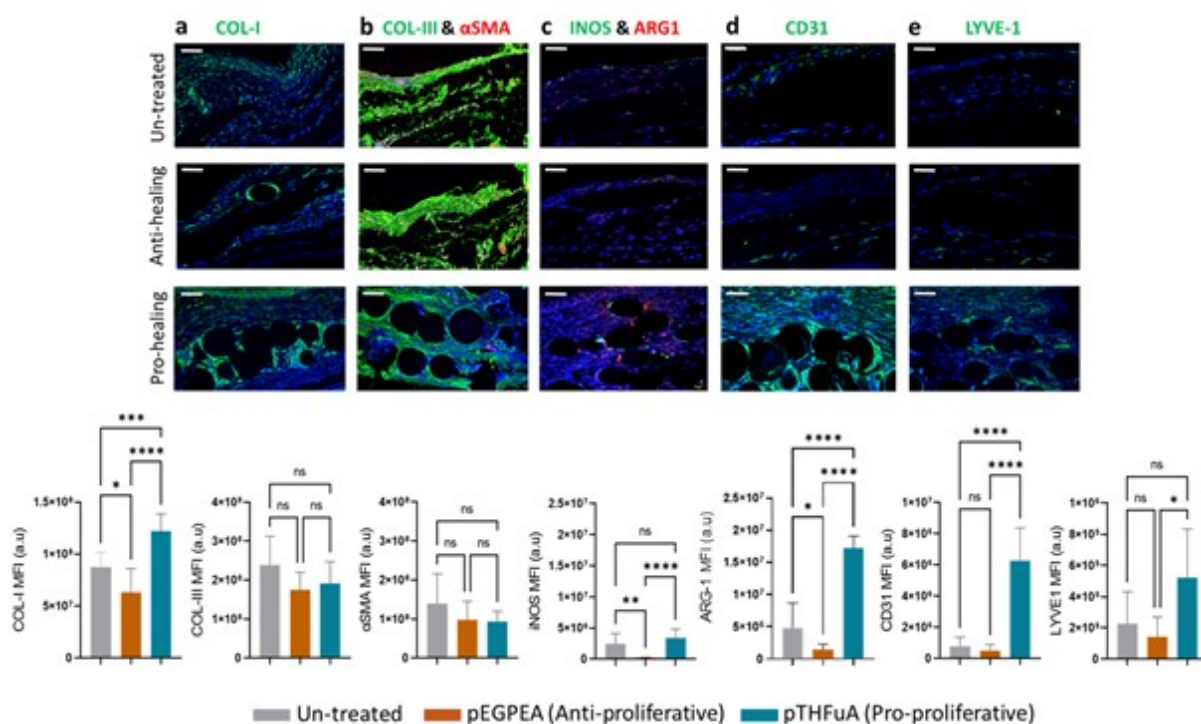
Figure 5. Immunofluorescence staining of tissues excised from diabetic mice treated with anti-proliferative (pEGPEA) and pro-proliferative (pTHFuA) microparticles. a) COL-1 (green) representative images and quantification. b) COL-3 (green) and α-SMA (red) representative images and quantification (green). c) iNOS (M1 marker green) and Arginase-1 (M2 marker red) representative images and quantification. d) CD31 (green) representative images and quantification. e) LYVE-1 (green). Scale bar = 50 μm. Images and quantifications are representative of *N*=8 *n*=5. Statistical significance was calculated using one-way ANOVA and the Tukey's post hoc analysis where *p <0.1, **p<0.01, ***p<0.001, ****p<0.0001.

To better understand whether the observed differential wound healing in response to different polymers is additionally driven in part via a change in neutrophil and macrophage infiltration and/or phenotype, this was evaluated *in vivo*. We observed higher numbers of macrophage (mostly of M2 phenotype) in tissues retrieved from diabetic wounds exposed to pro-proliferative microparticles. This is somewhat in contradiction with our *in vitro* data showing lower levels of MCP-1 (a monocyte chemoattractant) production by human fibroblasts cultured on pro-proliferative microparticles.

18

However, a diabetic wound environment is far more complex than reductionist *in vitro* experiments using fibroblasts only, and a host of other mediators[51] could be driving monocyte/macrophage infiltration in response to pro-proliferative microparticles *in vivo*. Interestingly, previous studies in diabetic mice have shown decreased macrophage numbers contribute to impaired diabetic wound healing.[52] We also find this to be the case upon application of anti-proliferative microparticles, whereas the pro-proliferative microparticles caused significantly higher infiltration of macrophages (p<0.0001) and neutrophils (p=0.0219) (Figure 4f and g). That said, even if pro-proliferative microparticles elicit an inflammatory response, it is not detrimental to wound closure. In fact, using iNOS as a M1 pro-inflammatory marker and Arg-1 as a M2 anti-inflammatory marker (Figure 5c), data shows macrophages in the wounds of diabetic mice treated with pro-proliferative microparticles had significantly increased anti-inflammatory expression levels compared to anti-proliferative microparticle addition (p<0.0001) and un-treated wounds (p<0.0001). Activated macrophages have also been reported to induce the formation of blood and lymphatic vessels via secretion of growth factors such as (VEGF)-A and -C.[53] Alongside this, delayed wound healing, has in part been related to reduced lymphatic development.[52] Quantitative evaluation of vascularity (Figure 5d) via CD31 immunostaining was significantly evidenced on wounds treated with pro-proliferative microparticles opposed to anti-proliferative (p<0.0001) and un-treated wounds (p<0.0001). LYVE-1 immunostaining for determination of lymphatic vessel development was also greatest from tissue retrieved from diabetic mice treated with pro-proliferative microparticles (Figure 5e), which coincides with a higher macrophage count (Figure 5f). In essence, the critical role of macrophages is demonstrated not only by their phenotype but also by the fact that their depletion in diabetic wounds and link to angiogenesis and lymphatic vessel formation, leads to a delay in wound healing.

In this study, a high-throughput screening approach successfully identified polymer chemistries that were able to modulate fibroblasts towards pro-and anti-proliferative phenotypes for application in a diabetic wound microenvironment. For a surface to have potential to bring about improved wound healing, chemical cues must instruct fibroblasts to attach, spread and proliferate whilst controlling differentiation to myofibroblasts. Myofibroblasts are involved in the inflammatory response to injury

WILEY-VCH

and produce and organize ECM needed to restore tissue integrity. Too many myofibroblasts working for too long however, can lead to fibrosis and scarring, whilst insufficient numbers prevents normal wound healing.[54] pTHFuA was found to increase cell proliferation whilst decrease differentiation to myofibroblasts, whilst pEGPEA decreased cell proliferation and increased differentiation. This behavior remained when the polymers were spin coated onto glass coverslips creating a macro-scale area as opposed to a polymer spot at micro-scale. *In-vitro* scratch assays also revealed that the pTHFuA (pro-proliferative polymer) accelerated wound healing compared to the pEGPEA (anti-proliferative polymer) and no treatment. Clearly using a different control substrate other than TCP could have potentially identified additional polymers with pro- or anti-proliferative properties. This will be considered in any future screening of this polymer library. Nevertheless, both *in vitro* and *in vivo* data conforms with the predicted bio-instructive potential of the selected hit polymers.

To create a format in which fibroblast instructive materials could be applied to a wound bed, polymer microparticles with pro- and anti-proliferative surface chemistries were fabricated using a droplet microfluidic process. Fibroblasts cultured on the pro-proliferative microparticles were shown to promote proliferation, modulate collagen synthesis, and regulate secretion of pro-proliferative/anti-inflammatory cytokines and growth factors. The application of pro-proliferative microparticles to diabetic wounds in rodents significantly improved the rate of wound healing and had a positive impact on neo-dermal tissue generation compared to anti-proliferative microparticles and un-treated wounds. Promotion of granulation tissue induced by the pro-proliferative microparticles was in part a result of increased cell proliferation and upregulation of COL I/COL III. MMP-1 production was also downregulated in these wounds compared to those treated with anti-proliferative particles. MMPs are a family of proteases that are capable of degrading various extracellular matrix protein including collagen, and have been shown to be increased due to sustained inflammation in wounds with impaired healing. By degrading ECM, reduced collagen expression (COL I/COL III) and GTD was evident in diabetic wounds treated with the anti-proliferative microparticles but not the pro-proliferative microparticles. We also investigated if immune cell infiltration, specifically macrophages, increased the efficacy of the pTHFuA polymer to induce improved wound healing. Increased numbers of macrophages in wound tissue exposed to pro-proliferative microparticles and decreased numbers upon exposure to the anti-proliferative

20

microparticles correlate with studies which show macrophage depletion at any stage of wound healing. With the exception of late stage (tissue maturation), which will result in significant impairment in vascularized granulation tissue formation, wound-re-epithelialization and closure.[55] Thus, high numbers of macrophages with an anti-inflammatory phenotype in mice exposed to pro-proliferative microparticles adds to the regenerative ability to bring about wound healing. Delayed wound healing, has also in part been related to reduced lymphatic development and angiogenesis, also found in this study.

The use of microparticles to promote wound healing has previously been reported. For example, negatively charged synthetic polystyrene microspheres (NCM) applied to patients with diabetic foot ulcers, have shown to promote neoangiogenesis and granulation tissue formation, thus wound healing.[56] Whilst this is promising, daily application of the NCM was required, making treatment expensive.[56] Our approach using microparticles decorated with cell-instructive polymers requires a single application to enhance healing of diabetic wounds by promoting wound closure rates, collagen deposition, angiogenesis, lymphatic vessel formation and enrichment of fibroblast and macrophage populations of the anti-inflammatory phenotype. This could prove beneficial in the care of chronic diabetic wounds where frequent wound dressing changes are required. Future investigation should focus on manufacturing the next generation of microparticles from a biodegradable core material utilising the functional surfactants developed within this paper, and validating the biocompatibility and diabetic wound healing efficacy in more extensive pre-clinical studies which most closely mirror the human wound healing process.[50]

3. Conclusion

The strategy of directing fibroblast functional phenotype using active bio-instructive microparticles towards distinct pro- and anti-proliferative phenotypes and behaviors is a novel approach of

harnessing the remodelling potential of these cells. Through screening an array of surface chemistries, we identified pTHFuA (pro-proliferative polymer), and successfully used the surfmer method to decorate microparticles to deliver bio-instructive polymer *in vivo* for the first-time. The pro-proliferative microparticles significantly promoted wound healing and tissue granulation compared to pEGPEA (anti-proliferative polymer) coated microparticles and un-treated wounds. A polymer-based solution to such an important clinical need that does not rely on delivering exogenous growth factors, cytokines or drugs, and critically does not require re-application, has not previously been reported and could offer exciting translational opportunities. Characterization of the wound microenvironment revealed combinations of collagen I and III along with MMP1 expression and functions of macrophages which led to granulation tissue formation, vascularisation and lymphatic vessel formation serving as major factors in driving pro- and anti-proliferative responses. Our results offer encouraging insights into the applicability of active non-eluting immune instructive polymer (pTHFuA) which supports diabetic wound healing and potential for translation to the clinic for treating diabetic wounds and potentially burn and other types of chronic or acute wounds.

4. Experimental Section

Polymer array synthesis

Polymer microarray were fabricated as previously described.[16, 57] In brief, polymer microarrays were printed onto epoxy coated slides (Xenopore) dip coated with poly (2-hydroxyethyl methacrylate) (pHEMA) (4% w/v, Sigma) in ethanol (95% v/v, in water). Monomers (Sigma Aldrich, Scientific Polymers and Polysciences) in polymerization solution were printed using a XYZ3200 dispensing station (Biodot) and metal pins (946MP6B, Arrayit). The polymerization solutions were composed of monomer (50% v/v) in dimethlyformamide with photoinitiator 2,2-dimethoxy-2-phenyl acetophenone (1% w/v). Three replicate spots were printed on each slide. The printing conditions were O_2 (< 2000 ppm), 25°C, and humidity (35%). To initiate polymerization, the arrays were

irradiated with UV (365nm) for 1 min immediately after printing and for an additional 10 min at the end of the print cycle. The arrays were sterilized with UV light for 20 minutes prior to cell culture.

Polymerization and spin coating scaled up coupon sized surfaces

α,α′-Azoisobutyronitrile (0.5 wt % to monomer) was added to a solution of degassed monomer (pro-proliferative: tetrahydrofurfuryl acrylate and anti-proliferative: ethylene glycol phenyl ether acrylate) under argon. The reaction mixture was then placed immediately into a preheated oil bath (80°C) and stirred for 18 h. The polymer solution was precipitated thrice by dropwise addition to stirred hexane at 4°C. The isolated, purified polymer was then stored under vacuum (<1 mbar) for 72 h before use to remove any remaining volatiles. Polymers (2% w/v in toluene) were spin coated (2000 rpm) for 30 seconds using spin coater (Mk7, Cordell group) on glass coverslips (13 mm). The coated surfaces were vacuum dried for 96 hours and placed in distilled water at 37°C for a further 48 hours to remove remaining volatiles, before sterilization with UV light and cell culture.

Microparticle Production

Equipment: Particles were synthesized using a droplet microfluidic system (TELOS, Dolomite UK), which enabled for the scale-out droplet microfluidic system with 7 droplet generators operating at once. A 100 μm hydrophilic Telos® 2 reagent chip SC (Dolomite, UK) was used to produce emulsions. 1.6 mm x 0.25 mm (Outer diameter x inner diameter) FEP tubing was used to connect pressure pumps to the droplet system and used as the outlet tubing to connect the droplet system to the collection vessel. Emulsions were solidified using a wavelength fibre optic (365 nm) and resulting particles were separated using nylon mesh (40 μm).

Surfmer Synthesis: The polymeric surfmers used in this present work were synthesized following a previously developed protocol[27]. Briefly the synthetic steps and characterization are reported below. A Chemspeed Swing robot (Chemspeed Technologies Pty Ltd.) equipped with an isynth

reactor containing 48 individual reactors was used for all polymerizations. For aspirations and dispensing of reagent solutions, a 4-Needle Head tool equipped with 2 x 1 mL and 2 x 10 mL syringes was used which was fitted with stainless steel septa piercing needles. All solvent lines were primed with degassed cyclohexanone which was used for each rinsing step. Typical aspiration and dispense rates of the reagents were 2 ml/min and 5 ml/min, for the 1 mL syringes and 10 ml/min and 5 ml/min, respectively. All reagents were added to the reactors including monomers (ThFuA, EGPEA and mPEGMA (MW: 300 g/mol) (Sigma Aldrich)), Bis[(difluoroboryl)diphenylglyoximato] cobalt (II) (PhCoBF, DuPont), initiator (2'-azobis (2-methylpropionitrile) (AIBN, 98%) and cyclohexanone (Fisher Scientific) prior to heating. The appropriate quantities of the monomers (ThFuA/EGPEA:mPEGMA) required to reach the targeted molar ratios (90/10 % mol/mol), were introduced into the required volume of cyclohexanone with stirring, such that a 1/3 v/v ratio mixture was achieved. The isynth reactor was kept under reflux conditions to obtain a temperature of 75°C inside the reactors for 18 hours. The isynth reactor was set to shake (400 rpm) for the duration of the polymerizations to ensure adequate mixing. It was then cooled to 20°C in order to cease the polymerizations. The purifications of the polymers were conducted in an excess of heptane. The usual non-solvent:reaction media ratio was 5:1 vol/vol in order to enhance the precipitation process and, finally, the precipitated materials were collected in a vial and left in vacuum oven for at least 24 hrs. ^{1}H-NMR spectroscopic analysis was performed on the crude polymerization solution to determine polymer conversion and, finally, on the precipitate to establish the actual monomer ratio of the final copolymer composition. To evaluate the molecular weight of the materials, the purified samples were dissolved in HPLC grade THF for GPC analysis. All the spectra data presented were collected at 400 MHz in CDCl3 and values are quoted as δH ppm.

The ^{1}H-NMR of THFuA-*co*-mPEGMA purified (400 MHz, CDCl$_3$) δ (ppm): 3.90-3.66 (3H, OCH$_2$CHO, m), 3.63-3.45 (4H, CHOCH$_2$ and C=OOCH$_2$ (mPEGMA), m), 3.43 (18H, C=OOCH$_2$CH$_2$O and (OCH$_2$CH$_2$O)$_4$, m), 3.14 (3H, OCH$_3$, s), 1.94-1.72 (3H, OCH$_2$CH$_2$CHH, m), 1.51 (1H, OCH$_2$CH$_2$CHH, m). M$_n$: 10 640 g/mol, Đ: 2.45, actual monomer ratio: 91/9 mol/mol THFuA/mPEGMA.

The ^{13}C-NMR of the THFuA-*co*-mPEGMA copolymer purified (400 MHz, CDCl$_3$) δ (ppm): 174 (C=O), 76.22 (CHOC$_3$H$_6$), 71.74 (CH$_2$OCH$_3$), 70.48 ((OCH2CH2)$_4$), 68.54 (OCH$_2$CH$_2$, OCH$_2$CH), 68.07 (OCH$_2$CH$_2$), 59.08 (OCH$_3$), 41.95 (CHOCH$_2$C$_2$H$_4$), 28.18 (CHOCH$_2$CH$_2$CH$_2$), 25.64 (CHOCH$_2$CH$_2$CH$_2$).

The ^{1}H-NMR of EGPEA-*co*-mPEGMA purified (400 MHz, CDCl$_3$) δ (ppm): 7.22 and 6.87 (5H, C$_5$H$_5$, m), 4.30 (4H, C=OOCH$_2$, m) 4.04 (2H, OCH$_2$CH$_2$, m), 3.60 (18H, CH$_2$CH$_2$O and (OCH$_2$CH$_2$)$_4$O, m), 3.40 (3H, OCH$_3$, m). M$_n$: 9 320 g/mol, Đ: 2.19, actual molar ratio: 89/11 mol/mol EGPEA/mPEGMA.

The ^{13}C-NMR of the EGPEA-*co*-mPEGMA purified (400 MHz, CDCl3) δ (ppm): 174 (C=O), 129, 121.13 and 114.46 (C$_6$H$_5$), 82.56 (OCHC$_9$H$_{12}$), 71.74 (CH$_2$OCH$_3$), 70.48 ((OCH$_2$CH$_2$)$_4$), 68.54 (OCH$_2$CH$_2$), 68.07 (OCH$_2$CH$_2$), 59.08 (OCH$_3$).

Chemicals and Flow Rates: The continuous phase throughout all experiments was DI water. The continuous phase was operated at a target flow rate of 420 µm/min. The dispersed phase comprised of: surfmer (2% w/v) and photoinitiator (2% w/v) (2,2 dimethoxy-2-phenylacetophenone) in hexanediol diacrylate (1.6). For experiments with no surfactant, no surfmer was added to the dispersed phase and instead ethyl acetate (10 % v/v) was added. All chemicals were used as received. The dispersed phase flow rate was operated at a target flow rate of 12 µm/min.

Characterization: Resultant microparticles were sized using a Hitachi TM3030 table-top SEM. Images were taken at x30, x150, x250 and x800 magnifications. Size analysis was performed on 3 regions of interest taken at the x150 magnification using Fiji Software. Surface analysis was conducted using a previously published method.[27] A ToF-SIMS IV instrument (IONTOF GmbH, Münster, Germany) using a 25 keV Bi$_3$$^+$ primary ion source was used for surface chemistry analysis. Bi$_3$$^+$ primary ions were used with a target current of ~0.3 pA. Analysis for positive and negative spectra was acquired over a 500 µm × 500 µm scan area. A cycle time of 100 µs, one shot/frame/pixel, one frame/patch and 20 scans per analysis was also used. As the samples were non-conductive, a charge compensation in the form of a low energy (20 eV) electron flood gun was applied. Images and spectra were acquired

WILEY-VCH

using SurfaceLab 6 software (IONTOF GmbH, Münster, Germany) and analyzed using SurfaceLab 7.1 software (IONTOF GmbH, Münster, Germany).[58]

The MFP-3D Standalone Atomic Force Microscope (AFM) (Oxford Instruments, Asylum Research Inc., CA) was used to obtain force-displacement curves of the polymer samples in water for Young's modulus calculation. Following data collection, the Derjaguin-Muller-Toporov mathematical model was used to fit the slope of the retracting curve using least squares regression line for calculation of Young's modulus.

Cell culture

The human lung fibroblasts (CCL-171, ATCC) and human skin fibroblasts (CRL-2522, ATCC) were cultured in Minimum Essential Medium Eagles (MEM) supplemented with fetal bovine serum (10% FBS), L-glutamine (1%), non-essential amino acids, penicillin/streptomycin and sodium pyruvate (Sigma). The cells were cultured in T75 flasks at 37°C with supplemental CO_2 (5%) until 90% confluent before passaging and/or seeding.

Immunostaining of fibroblasts on polymer arrays and spin coated films

Cells were fixed and permeabilized with triton-x (0.15% Sigma). To fluorescently stain for F-actin the cells incubated with Alexa Fluor 647 Phalloidin (1:50 dilution Cell Signaling Technology) for 30 minutes. The nuclei were stained with 4',6-diamidino-2-phenylindole (DAPI, Sigma). Cell attachment was measured by counting number of nuclei and cell size quantified by measuring cytoskeletal area. Cell proliferation on the polymer array was quantified by counting number of nuclei at 24 hours and 96 hours of culture. To probe for α-SMA the cells were fixed and permeabilized with triton-x (0.5% Sigma). Non-specific binding proteins were blocked with goat serum (10%) for 30 minutes. The cells were then treated with anti α-SMA (Sigma) and Rhodamine Red - X (Thermofisher Scientific) was used as a secondary antibody. Cell proliferation on scaled up polymer films was measured with the

Baseclick EdU imaging kit (Baseclick). EdU was added to cell medium (3 µM) at 72 hours of culture, where it was incorporated into newly synthesized DNA during the G1/S phase of the cell cycle. After 24 hours, the cells were fixed and stained for EdU following manufacturer's instructions. Polymer arrays and coated polymer films were imaged using the Zeiss TIRF (Carl Zeiss) device in widefield mode with a 20x air objective. Image analysis routines were developed to count cell nuclei, measure cell area and mean fluorescence intensity on FIJI.

Wound healing assay

In vitro wound assays were performed using IBIDI self-culture inserts. The IBIDI self-culture inserts were used to form wells on TCP, pro- and anti-proliferative polymer films. Briefly, when confluent layer of cells was formed, the insert was removed, and cells washed twice with PBS. The wounded monolayers were then cultured in complete medium for up to 96 hours. The samples were fixed and stained with anti α-tubulin (Abcam), and conjugated with Texas Red - X (Thermofisher Scientific). Cell proliferation was studied by measuring the number of Edu positive cells as previously described. Samples were measured on the Zeiss TIRF (Carl Zeiss) device in widefield mode. Wound closure was calculated by measuring area covered by cells within the wounded area at 0 hours, 48 hours, and 96 hours.

Fibroblast attachment and proliferation on microparticles

Cell attachment and proliferation of fibroblasts on microparticles was measured using the CyQuant™ NF assay (ThermoFisher) at 24 hours and 96 hours of culture. This method is based on measurement of cellular DNA content via fluorescent dye binding, where the cellular DNA content is proportional to the number of cells. The DNA content of fibroblasts cultured on microparticles was measured and their fluorescence intensity was compared against fluorescence intensity of known cell seeding densities.

WILEY-VCH

Cytokine quantification assay

The concentrations of bFGF, IL-6, HGF, IL-6, MCP-1, and TGF-β1 secreted into the medium by fibroblasts cultured on microparticles was analyzed after 96 hours of culture with Duoset ELISA kits (R&D Systems) according to manufacturer's instructions. The concentrations of MMP-1 and MMP-3 were measured using Eve Technologies custom-plex Multiplexing Bead assay (Eve technologies corporation, Canada) as described previously.[59]

RT-PCR

Total RNA was isolated from cells using RNeasy plus kit (Qiagen) followed by cDNA synthesis using a qPCRBIO cDNA synthesis kit (PCR Biosystems). Real-time PCR was performed on the MxPro 3005P qRT-PCR system (Stratagene, USA) using 2x qPCRBIO SyGreen Blue mix Lo-Rox (PCR Biosystems), according to manufacturer's instructions. Forward and reverse primers were purchased from Eurofins Scientific UK and Sigma, these are listed in Table 1. Gene expression levels were first normalized to housekeeping gene, glyceraldehyde-3-phosphate dehydrogenase (GAPDH), and then the relative expression levels were calculated with the $2^{-\Delta ct}$ method.

Table 1. Primers for fibroblast ECM markers used in real-time qPCR

Genes	Primer	Sequence (5'-3')
GAPDH	Forward	ACAGTCCATGCCATCACTGCC
	Reverse	GCCTGCTTCACCACCTTCTTG
Collagen I (α1)	Forward	GTCGCACTGGTGATGCTG
	Reverse	GGTGGTGTCCACCTCGAG
Collagen III (α1)	Forward	AGCTGGAAAGAGTGGTGACAG
	Reverse	CCTTGAGGACCAGGAGCAC

The db/db diabetic mouse model

Wound healing studies were carried out by CicaBiomedical Ltd. 32 male, 9 week old diabetic mice (BKS.Cg-m Dock7^m +/+ Lepr^{db} /J, Stock Code 00642, Jax, USA), were used in the study and all animal procedures carried out in a Home Office licensed establishment under Home Office Licences (PCD: 50/2505; PPL: P81E9540D; PIL: IBCEFDF55; PIL: I34817249). Mice were acclimatised to their surroundings for 7 days according to Home Office regulations and specific requirements of diabetic animals. Food (Standard Rodent Diet) and water were provided *ad libitum*. Animals were randomly allocated to one of 3 treatment regimens: 1. Un-treated (no particles) *N*=8, 2. Anti-proliferative coated particle addition *N*=8 and 3. Pro-proliferative coated particle addition *N*=8. On day 0, mice were anaesthetised (isofluorane & air) and the dorsum shaved and cleaned with chlorhexidine gluconate (0.5% w/v in 70% IMS VetaSept). Wound sites were swabbed with IMS (70%), and a single standardised full-thickness wound (10.0 mm x 10.0 mm) created in the left dorsal flank skin of each experimental animal. After experimental wounding, animals were housed in individual cages (cage size 500 cm^2 with sawdust bedding, changed three times per week), in an environment maintained at an ambient temperature of 23°C with 12 hour light/dark cycles and given analgesia (Vetergesic, [buprenorphine]) after surgery and as required. Animals received prophylactic antibiotics (in the form of Enrofloxacin [Baytril], subcutaneous (s.c)) on the day of wounding and subsequently on every 4th post-operative day. Functionalized and non-functionalized microsphere formulations (3.2 mg) were applied to the surface of wounds and distributed evenly using a sterile spatula. Wounds were then dressed with transparent film dressing Tegaderm™ Film (3M Deutschland GmbH, Germany) and physiological saline (40 µL) injected through the dressing onto the particles. Animals were allowed to recover under warmed conditions their health status monitored on a daily basis throughout the study. All wounds were digitally photographed at day 0 of wounding and on post-wounding days 4, 8, 12, 16 and 20 all mice were re-anaesthetised, wounds assessed and digitally photographed over time. Animals were given time to recover under warmed conditions after each anaesthetic episode. One hour prior to termination all animals received an i.p. injection (30 µg/g) of 5-bromo-2'-deoxyuridine (Sigma, B5002) for future assessment of cellular proliferation. On post-wounding day 20, animals were painlessly killed by a UK Home Office compliant method. Wounds

and surrounding normal tissue were excised, fixed in 10% buffered formalin (Sigma, UK), processed and embedded in paraffin wax. Wound healing assessment was carried out blindly and revealed at the end.

Wound healing assessment

Image Pro Plus analysis software (version 4.1.0.0, Media Cybernetics, USA) was used to calculate wound closure from scaled wound images taken over the 20 day period and expressed in terms of % wound area relative to day 0. As the process of wound closure results from the combined effects of wound contraction (the inward movement of marginal tissue) and re-epithelialization (wound resurfacing by the inward the migration of epithelial cells), wound closure over time was also considered with respect to these components. Wound contraction over time was determined by the difference between the contracted wound area at a given time point and the original wound area, and expressed as a percentage of the original wound area. Re-epithelialization over time was determined by taking the contracted wound area at a given time and subtracting it from the open wound area at that given time, and expressing it as a % of the original wound area. Initiation of healing was assessed in all wounds in the study on a daily basis until day 8 and subsequently on alternate days until day 20 to establish their healing status. Each wound was scored as to whether it was displaying neo-dermal tissue generation activity. Scoring was undertaken by two independent observers and the average % of wounds displaying neo-dermal tissue generation activity was compared between treatment groups at each assessment point. Neo-dermal tissue formation was considered to have started when blood vessels within the fascia of the wound base were concealed by overlying material, invariably the formation of a reddish exudate within the wound void.

Histology

Wax embedded tissues were sectioned (7 μm), stained with Haematoxylin and Eosin (H&E) and digitally scanned to determine the impact of the microparticle coatings on granulation tissue formation and re-epithelialization at the histological level. Granulation tissue deposition was

measured in terms of granulation tissue depth using QuPath image analysis software. A region of interest (ROI) was drawn onto the histology scan occupied by granulation tissue and particles. The ROI was thresholded for granulation tissue, and the area (in μm^2) of the ROI occupied by granulation tissue was determined. Areas occupied by particles were disregarded. The wound width, taken as the distance between hair bulbs (in µm) was determined and the average granulation tissue depth for each section calculated by dividing granulation area by wound width.

The extent of re-epithelialization from the left and right margins of each wound were measured from H&E-stained sections using Aperio ImageScope image analysis software (Leica Biosystems, UK). Wound re-epithelialzsation was expressed as the percentage of the wound surface epithelialized. H&E stains were also used to visually quantify macrophage and neutrophil infiltration. Counts were taken from three different locations across the tissue bed of each section (N=8, n=3). In addition tissue sections were stained with Massons Trichrome (Sigma) and visualised on a Zeiss Axioplan light microscope with digital image capture and analysis to determine collagen thickness. Collagen thickness was measured using Image J software at three region of interests per tissue section across the wound bed and expressed as average collagen thickness in µm.

Immunohistochemistry

Immunofluorescence staining was used to determine collagen I, collagen III, α-SMA, CD31 and LYVE-1 expression, and macrophage phenotype (iNOS - pro-inflammatory (M1) marker and Arginase-1 - anti-inflammatory (M2) marker). Antigen retrieval was carried out by heating (100°C) tissue sections for 20 min in citrate buffer (pH 6). Cells were permeabilized using triton X100 (0.5%) for 10 min and rinsed 3X5 min in PBS Tween 20 (0.2%). Non-specific binding was blocked by incubating tissue sections in BSA (5%) with donkey serum (5%) for 1 h at room temperature. Single or dual antibody staining was undertaken using: rabbit anti-mouse Collagen I (1;100; NB300-408 Novus Biologicals), rabbit anti-mouse Collagen III (1:100; NB600-594 Novus Biologicals), goat anti-mouse Smooth muscle actin (1:100; NB300-978 Novus Biologicals), rabbit anti-mouse CD31 (1:400; GTX130274 GeneTex), rabbit anti-mouse LYVE1 (1:500; NB600-1008 Novus Biologicals), rabbit anti-

WILEY-VCH

mouse iNOS (1:50; ab15323 Abcam) and goat anti-mouse Arg-1 (1:50; PA5-18392 ThermoFisher Scientific) antibodies and incubating at 4°C overnight. Secondary antibodies included donkey anti-goat IgG (H+L) and donkey anti-rabbit IgG (H+L) labelled with Alexa Fluor 594 and 488 (1:500; A11058 and A21206 ThermoFisher Scientific) respectively, were applied for 1 h at room temperature, followed by counterstaining with DAPI. Five images *(n*=5) per tissue section (*N*=8) were acquired on a Zeiss LSM880C confocal microscope and the mean fluorescence intensity density of each scan spanning the whole wound bed area (excluding far edges) was quantified using Image J software. Secondary only antibodies served as controls and background autofluorescence was subtracted. BrdU uptake by proliferating cells were detected by immunostaining for BrdU (1:500; ab152095 Abcam) in tandem with standard ABComplex immunoperoxidase detection techniques (VECTASTAIN Elite ABC-HRP Kit, Peroxidase Rabbit IgG, PK-6101 Vector Laboratories). Briefly, cells were permeabilized using triton X100 (0.5%), rinsed 2X5 min in PBS prior to being blocked for endogenous peroxidase using H_2O_2 (3%). Non-specific binding was blocked with normal blocking serum for 1 hour and the BrdU primary antibody incubated overnight at 4°C. Diluted biotinylated secondary antibody was added to sections as appropriate for 1 hour followed by ABC reagent for a further hour. ImmPACT DAB Substrate (SK4105 Vector Laboratories) was used as the detection reagent and tissues were counterstained with Harris haematoxylin (Sigma) prior to mounting with VectaMount mounting medium (H5000-60 Vector Laboratories). Slides were viewed on a Zeiss Axioplan light microscope and five images per tissue section captured. Proliferating cells were counted in three region of interests per image covering the wound bed area (excluding far edges). MMP-1 (1:500; GTX100534 GeneTex) expressing cells were also detected and quantified using this method.

Statistical analysis

High throughput screening data was pre-processed by normalizing to TCP controls. All data acquisitioned is expressed as mean ± standard deviation. Biological (*N*) and technical (*n*) replicates are supplied in the relevant methods sections. Use of statistical significance was calculated using one-way ANOVA and the Tukey's post hoc analysis on GraphPad Prism 8, whereby p ≤ 0.1 was considered as being statistically significant.

WILEY-VCH

Supporting Information

Supporting Information is available from the Wiley Online Library or from the author.

Conflict of Interest

The authors declare no conflict of interest.

Data Availability Statement

All data are included in the article and/or supporting information. The data that supports the findings of this study can be found in the University of Nottingham data repository at https://rdmc.nottingham.ac.uk.   DOI: 10.17639/nott.7253

WILEY-VCH

References

[1]   S. A. Eming, T. Krieg, J. M. Davidson, *The Journal of investigative dermatology.* **2007**, *127*, 514.

[2]   M. Rodrigues, N. Kosaric, C. A. Bonham, G. C. Gurtner, *Physiological reviews.* **2019**, *99*, 665.

[3]   R. T. Kendall, C. A. Feghali-Bostwick, *Frontiers in Pharmacology.* **2014**, *5*.

[4]   P. Martin, R. Nunan, *The British journal of dermatology.* **2015**, *173*, 370.

[5]   H. E. Talbott, S. Mascharak, M. Griffin, D. C. Wan, M. T. Longaker, *Cell stem cell.* **2022**, *29*, 1161.

[6]   S. Patel, S. Srivastava, M. R. Singh, D. Singh, *Biomedicine & Pharmacotherapy.* **2019**, *112*, 108615.

[7]   E. Santos-Vizcaino, A. Salvador, C. Vairo, M. Igartua, R. M. Hernandez, L. Correa, S. Villullas, G. Gainza, *Nanomaterials (Basel, Switzerland).* **2020**, *10*.

[8]   Y. Huang, T. R. Kyriakides, *Matrix Biology Plus.* **2020**, *6-7*, 100037.

[9]   A. G. Maione, A. Smith, O. Kashpur, V. Yanez, E. Knight, D. J. Mooney, A. Veves, M. Tomic-Canic, J. A. Garlick, *Wound repair and regeneration : official publication of the Wound Healing Society [and] the European Tissue Repair Society.* **2016**, *24*, 630.

[10]   L. Yang, S. Pijuan-Galito, H. S. Rho, A. S. Vasilevich, A. D. Eren, L. Ge, P. Habibović, M. R. Alexander, J. de Boer, A. Carlier, P. van Rijn, Q. Zhou, *Chemical Reviews.* **2021**, *121*, 4561.

[11]   A. J. Vegas, O. Veiseh, J. C. Doloff, M. Ma, H. H. Tam, K. Bratlie, J. Li, A. R. Bader, E. Langan, K. Olejnik, P. Fenton, J. W. Kang, J. Hollister-Locke, M. A. Bochenek, A. Chiu, S. Siebert, K. Tang, S. Jhunjhunwala, S. Aresta-Dasilva, N. Dholakia, R. Thakrar, T. Vietti, M. Chen, J. Cohen, K. Siniakowicz, M. Qi, J. McGarrigle, A. C. Graham, S. Lyle, D. M. Harlan, D. L. Greiner, J. Oberholzer, G. C. Weir, R. Langer, D. G. Anderson, *Nature biotechnology.* **2016**, *34*, 345.

[12]   H. M. Rostam, L. E. Fisher, A. L. Hook, L. Burroughs, J. C. Luckett, G. P. Figueredo, C. Mbadugha, A. C. K. Teo, A. Latif, L. Kämmerling, M. Day, K. Lawler, D. Barrett, S. Elsheikh, M. Ilyas, D. A. Winkler, M. R. Alexander, A. M. Ghaemmaghami, *Matter.* **2020**.

[13]   A. D. Celiz, J. G. Smith, R. Langer, D. G. Anderson, D. A. Winkler, D. A. Barrett, M. C. Davies, L. E. Young, C. Denning, M. R. Alexander, *Nature materials.* **2014**, *13*, 570.

WILEY-VCH

[14]   A. Nasir, J. Thorpe, L. Burroughs, J. Meurs, S. Pijuan-Galito, D. J. Irvine, M. R. Alexander, C. Denning, *Adv Healthc Mater.* **2021**, *10*, 2001448.

[15]   A. D. Celiz, J. G. Smith, A. K. Patel, A. L. Hook, D. Rajamohan, V. T. George, L. Flatt, M. J. Patel, V. C. Epa, T. Singh, R. Langer, D. G. Anderson, N. D. Allen, D. C. Hay, D. A. Winkler, D. A. Barrett, M. C. Davies, L. E. Young, C. Denning, M. R. Alexander, *Advanced materials (Deerfield Beach, Fla.).* **2015**, *27*, 4006.

[16]   A. L. Hook, C.-Y. Chang, J. Yang, J. Luckett, A. Cockayne, S. Atkinson, Y. Mei, R. Bayston, D. J. Irvine, R. Langer, D. G. Anderson, P. Williams, M. C. Davies, M. R. Alexander, *Nature biotechnology.* **2012**, *30*, 868.

[17]   C. A. Henshaw, A. A. Dundas, V. Cuzzucoli Crucitti, M. R. Alexander, R. Wildman, F. Rose, D. J. Irvine, P. M. Williams, *Molecules.* **2021**, *26*.

[18]   A. A. Dundas, V. Cuzzucoli Crucitti, S. Haas, J.-F. Dubern, A. Latif, M. Romero, O. Sanni, A. M. Ghaemmaghami, P. Williams, M. R. Alexander, R. Wildman, D. J. Irvine, *Advanced Functional Materials.* **2020**, *30*, 2001821.

[19]   M. B. Oliveira, J. F. Mano, *Biotechnology progress.* **2011**, *27*, 897.

[20]   M. D. Neto, M. B. Oliveira, J. F. Mano, *Trends in biotechnology.* **2019**, *37*, 1011.

[21]   E. Tamariz, F. Grinnell, *Molecular biology of the cell.* **2002**, *13*, 3915.

[22]   J. Sapudom, X. Wu, M. Chkolnikov, M. Ansorge, U. Anderegg, T. Pompe, *Biomater Sci.* **2017**, *5*, 1858.

[23]   F. Strutz, M. Zeisberg, A. Renziehausen, B. Raschke, V. Becker, C. van Kooten, G. Müller, *Kidney international.* **2001**, *59*, 579.

[24]   A. C. Midgley, M. Rogers, M. B. Hallett, A. Clayton, T. Bowen, A. O. Phillips, R. Steadman, *The Journal of biological chemistry.* **2013**, *288*, 14824.

[25]   R. Wan, J. P. Weissman, K. Grundman, L. Lang, D. J. Grybowski, R. D. Galiano, *Wound repair and regeneration : official publication of the Wound Healing Society [and] the European Tissue Repair Society.* **2021**, *29*, 573.

[26]   A. Hüsler, S. Haas, L. Parry, M. Romero, T. Nisisako, P. Williams, R. D. Wildman, M. R. Alexander, *RSC Advances.* **2018**, *8*, 15352.

WILEY-VCH

[27]   V. Cuzzucoli Crucitti, L. Contreas, V. Taresco, S. C. Howard, A. A. Dundas, M. J. Limo, T. Nisisako, P. M. Williams, P. Williams, M. R. Alexander, R. D. Wildman, B. W. Muir, D. J. Irvine, *ACS Applied Materials & Interfaces.* **2021**, *13*, 43290.

[28]   S. ten Klooster, S. Sahin, K. Schroën, *Sci Rep.* **2019**, *9*, 7820.

[29]   D.-Y. Kim, S. H. Jin, S.-G. Jeong, B. Lee, K.-K. Kang, C.-S. Lee, *Sci Rep.* **2018**, *8*, 8525.

[30]   J. M. Rawlins, W. L. Lam, R. O. Karoo, I. L. Naylor, D. T. Sharpe, *Journal of burn care & research : official publication of the American Burn Association.* **2006**, *27*, 60.

[31]   D. Akilbekova, K. M. Bratlie, *PloS one.* **2015**, *10*, e0130386.

[32]   A. Bachhuka, J. Hayball, L. E. Smith, K. Vasilev, *ACS Applied Materials & Interfaces.* **2015**, *7*, 23767.

[33]   U. Klinge, Z. Y. Si, H. Zheng, V. Schumpelick, R. S. Bhardwaj, B. Klosterhalfen, *European surgical research. Europaische chirurgische Forschung. Recherches chirurgicales europeennes.* **2000**, *32*, 43.

[34]   T. Leavitt, M. S. Hu, C. D. Marshall, L. A. Barnes, H. P. Lorenz, M. T. Longaker, *Cell and tissue research.* **2016**, *365*, 483.

[35]   X. Yi, X. Li, Y. Zhou, S. Ren, W. Wan, G. Feng, X. Jiang, *Int J Mol Med.* **2014**, *34*, 381.

[36]   E. B. Jude, R. Blakytny, J. Bulmer, A. J. M. Boulton, M. W. J. Ferguson, *Diabetic Medicine.* **2002**, *19*, 440.

[37]   A. J. Cowin, N. Hatzirodos, C. A. Holding, V. Dunaiski, T. E. Rayner, R. H. Harries, R. Fitridge, R. D. Cooter, G. S. Schultz, D. A. Belford, *Journal of Investigative Dermatology.* **2001**, *117*, 1282.

[38]   E. H. Budi, J. R. Schaub, M. Decaris, S. Turner, R. Derynck, *The Journal of pathology.* **2021**, *254*, 358.

[39]   M. Muller, C. Trocme, B. Lardy, F. Morel, S. Halimi, P. Y. Benhamou, *Diabetic medicine : a journal of the British Diabetic Association.* **2008**, *25*, 419.

[40]   B. K. Pilcher, J. A. Dumin, B. D. Sudbeck, S. M. Krane, H. G. Welgus, W. C. Parks, *J Cell Biol.* **1997**, *137*, 1445.

[41]   S. M. Ayuk, H. Abrahamse, N. N. Houreld, *Journal of Diabetes Research.* **2016**, *2016*, 2897656.

[42]   T. T. Nguyen, M. Mobashery, C. Chang, *Roles of Matrix Metalloproteinases in Cutaneous Wound Healing*, 2016.

WILEY-VCH

[43]   P. Chomarat, J. Banchereau, J. Davoust, A. Karolina Palucka, *Nature immunology.* **2000**, *1*, 510.

[44]   K. P. Sundararaj, D. J. Samuvel, Y. Li, J. J. Sanders, M. F. Lopes-Virella, Y. Huang, *The Journal of biological chemistry.* **2009**, *284*, 13714.

[45]   K. Kawai, S. Suzuki, Y. Tabata, Y. Nishimura, *British journal of plastic surgery.* **2005**, *58*, 1115.

[46]   G. Ramanathan, S. Thyagarajan, U. T. Sivagnanam, *Materials Science and Engineering: C.* **2018**, *93*, 455.

[47]   M. Bahadoran, A. Shamloo, Y. D. Nokoorani, *Sci Rep.* **2020**, *10*, 7342.

[48]   P. Losi, E. Briganti, C. Errico, A. Lisella, E. Sanguinetti, F. Chiellini, G. Soldani, *Acta biomaterialia.* **2013**, *9*, 7814.

[49]   T. Wang, Q. Gu, J. Zhao, J. Mei, M. Shao, Y. Pan, J. Zhang, H. Wu, Z. Zhang, F. Liu, *Int J Clin Exp Pathol.* **2015**, *8*, 6636.

[50]   G. Theocharidis, H. Yuk, H. Roh, L. Wang, I. Mezghani, J. Wu, A. Kafanas, M. Contreras, B. Sumpio, Z. Li, E. Wang, L. Chen, C. F. Guo, N. Jayaswal, X.-L. Katopodi, N. Kalavros, C. S. Nabzdyk, I. S. Vlachos, A. Veves, X. Zhao, *Nature biomedical engineering.* **2022**.

[51]   P. Krzyszczyk, R. Schloss, A. Palmer, F. Berthiaume, *Frontiers in physiology.* **2018**, *9*, 419.

[52]   K. Maruyama, J. Asai, M. Ii, T. Thorne, D. W. Losordo, P. A. D'Amore, *The American journal of pathology.* **2007**, *170*, 1178.

[53]   Y.-K. Hong, B. Lange-Asschenfeldt, P. Velasco, S. Hirakawa, R. Kunstfeld, L. F. Brown, P. Bohlen, D. R. Senger, M. Detmar, *The FASEB Journal.* **2004**, *18*, 1111.

[54]   B. Hinz, *Current research in translational medicine.* **2016**, *64*, 171.

[55]   T. Lucas, A. Waisman, R. Ranjan, J. Roes, T. Krieg, W. Müller, A. Roers, S. A. Eming, *Journal of immunology (Baltimore, Md. : 1950).* **2010**, *184*, 3964.

[56]   J. L. Lázaro-Martínez, Y. García-Álvarez, F. J. Álvaro-Afonso, E. García-Morales, I. Sanz-Corbalán, R. J. Molines-Barroso, *Journal of wound care.* **2019**, *28*, 104.

[57]   D. G. Anderson, S. Levenberg, R. Langer, *Nature biotechnology.* **2004**, *22*, 863.

[58]   A. A. Dundas, S. Kern, V. Cuzzucoli Crucitti, D. J. Scurr, R. Wildman, D. J. Irvine, M. R. Alexander, *Surface and Interface Analysis.* **2022**, *54*, 374.

[59]   S. Y. Lim, J. H. Lee, S. J. Welsh, S. B. Ahn, E. Breen, A. Khan, M. S. Carlino, A. M. Menzies, R. F. Kefford, R. A. Scolyer, G. V. Long, H. Rizos, *Biomarker Research.* **2017**, *5*, 32.
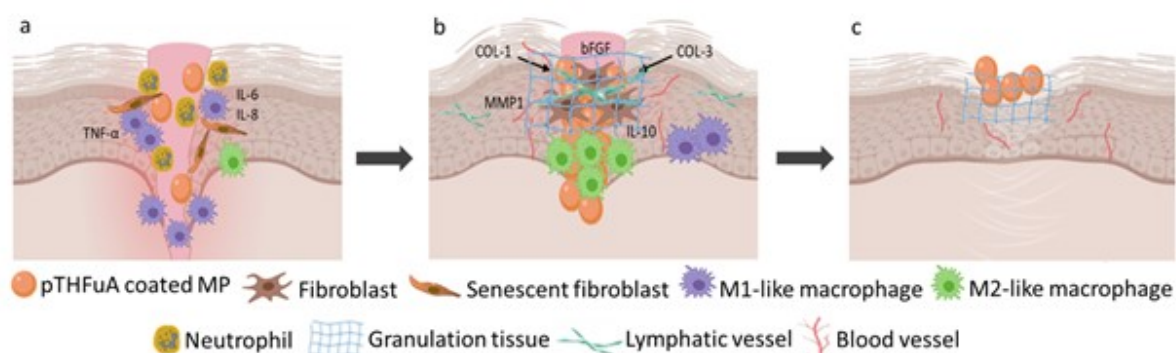
WILEY-VCH

Microparticles decorated with cell-instructive surface chemistries actively promote wound healing

Single application of pTHFuA decorated microparticles to wound beds in a full thickness diabetic wound model promoted almost complete healing and tissue granulation. The wound closure, granulation tissue formation and neovascularization are through active instruction of fibroblasts and macrophages towards pro-healing phenotypes as evidenced by changes in collagen deposition, MMP expression profile and cytokine environments.

Schematic showing:

a) Application of pTHFuA coated microparticles into diabetic wound bed. b) Microenvironmental shift towards accelerated healing. c) Tissue regeneration and healing. Created in BioRender.com.